AIAA JOURNAL
Vol. 47, No. 10, October 2009

Computations of Flow Past a Circular Cylinder Using a Continuous-Turbulence Model

Hongwu Zhao,* Ali Uzun,† and M. Y. Hussaini‡
Florida State University, Tallahassee, Florida 32306
and
Stephen L. Woodruff§
Florida State University, Tallahassee, Florida 32310

DOI: 10.2514/1.42927

A continuous Reynolds-averaged Navier–Stokes large-eddy-simulation turbulence model is derived based on the Kolmogorov universal energy scaling law in this study. With the continuous model, the eddy-viscosity for small-scale modeling is calculated with Reynolds-averaged Navier–Stokes equations using a function that is uniquely determined by the ratio of the resolved small-scale length to the integral length scale. The unified treatment of Reynolds-averaged Navier–Stokes large eddy simulation could be achieved with this continuous model by controlling the coarseness of the mesh. The continuous Reynolds-averaged Navier–Stokes large eddy-simulation model is initially tested with flow past a circular cylinder at the Reynolds number $Re = 3900$. Both constant integral length scales and varied integral length scales based on the mixing length are used in the simulations. The mesh dependence is also studied with both coarse and fine meshes. The comparisons are made and analyzed between the results with different integral length scales and different mesh sizes. These results are also compared with the experimental results and Reynolds-averaged Navier–Stokes results. The results demonstrate that with the continuous modeling, the large eddy-simulation-like simulation can be achieved by solving Reynolds-averaged Navier–Stokes equations alone. The spatially varied integral length scale is necessary to capture the more accurate turbulence quantities for anisotropic wall-bounded turbulent flow.

I. Introduction

SIMULATION of turbulent flows at high Reynolds numbers is an important but difficult issue in engineering analysis and design. Because direct numerical simulation (DNS) is impractical for most turbulent flows with even the fastest computers today, turbulence modeling is the only way to resolve the dilemma between computational cost and accuracy. Reynolds-averaged Navier–Stokes (RANS) computation and large eddy simulation (LES) are the main approaches to turbulence simulations with turbulence models [1,2]. In LES, the dynamics of the larger turbulence length scales are resolved numerically and the small scales are modeled. The vast majority of LES computations make use of eddy-viscosity based subgrid-scale models in conjunction with the spatially averaged Navier–Stokes equations. In this approach, the effect of the unresolved turbulence is modeled as an effective increase in molecular viscosity. On the other hand, RANS equations are obtained by time-averaging the Navier–Stokes equations. Most of the unsteadiness is averaged out and the temporal mean quantities are resolved numerically while the remaining unsteadiness is modeled. RANS simulations are more affordable than LES; however, their accuracy is limited and they fail to provide unsteady and statistical information required in many applications.

The fact that even LES is still computationally prohibitive for many complex flows of engineering interest (jet and cavity acoustics, for example) has led to interest in hybrid LES–RANS techniques. In these techniques, LES modeling and fine-grid resolutions are employed only in those parts of the flow domain in which it is required to capture the unsteady behavior of the flow and to compute accurate statistics. RANS modeling and coarser-grid resolutions are employed in the remainder of the flow, enabling considerable savings in computational cost. For this purpose, the zonal RANS–LES techniques have been employed in some engineering applications [3–7]. In the zonal approach, LES is only applied in the most important regions of interest to capture the small scales. In these areas, the mesh is refined for the LES application. RANS is applied in areas in which the small scales are not so important and a statistically averaged flowfield is enough for engineering design and analysis. In these areas, relatively coarse grids are used for RANS. The zonal RANS–LES technique has proven to be an effective approach for both increasing simulation accuracy and decreasing computational cost. However, the so-called restriction-and-reconstruction procedure to treat the zonal interface region between RANS and LES is difficult to implement in simulations involving complex geometries, and it is the most challenging issue in this approach. Moreover, in aeroacoustic simulations with high-order numerical schemes, acoustic waves may reflect from the zonal interface and cause numerical errors. To remedy the eddy-viscosity discontinuity problem at the interface between RANS and LES zones, the RANS equations must also be solved in the LES zone. This entails extra computational expense. Because of all of these issues, the application of the zonal RANS–LES approach is limited.

The defects of the zonal RANS–LES approach may be overcome through the use of a continuous-modeling technique. The main idea of this concept is to realize a smooth transition from RANS to LES. The unified RANS–LES equations are solved to obtain the eddy viscosity. The extent of the resolved scales depends on the mesh cutoff scale relative to the characteristic large scale of the turbulence. Therefore, in the coarse-mesh region, fewer turbulence scales are resolved and RANS simulation is achieved. When the mesh is finer, a larger range of turbulence scales are resolved and LES is achieved. A smooth transition between RANS and LES takes place as the mesh resolution smoothly changes from coarse to fine, eliminating the difficulties mentioned previously that are associated with

Received 24 December 2008; accepted for publication 12 May 2009.

*Postdoctoral Research Associate, School of Computational Science.
†Research Associate, School of Computational Science. Senior Member AIAA.
‡Sir James Lighthill Professor, School of Computational Science. Fellow AIAA.
§Research Scientist, Center for Advanced Power Systems.

discontinuities in the mesh and the eddy viscosity. Additional computational savings may be achieved through use of a computationally simpler pure subgrid-scale model in those regions of the flow that are fully in the LES regime. Spalart [8], Spalart et al. [9], and Spalart [10] were among the first to have employed the continuous-modeling idea in the derivation of the detached eddy simulation (DES) approach, wherein a RANS simulation is performed inside the boundary layer and an LES-like simulation is performed in the far wake. The DES method requires careful mesh adaptation in the so-called gray area between RANS and LES [11]. Speziale [12] proposed an ad hoc equation for continuous-turbulence modeling. He introduced a factor, which is an exponential function of grid size, to rescale the RANS eddy viscosity to achieve LES in the fine-mesh region. More recently, a more rational continuous-modeling approach has been pursued by Hussaini et al. [13]. They obtained, among other functional forms, an exponential function similar to Speziale's [12] original function. The simulations performed with the new function showed the effectiveness of this approach for Kolmogorov flows. However, the assumptions made in their derivation need further validation. There are other coupled RANS–LES approaches discussed by Sagaut et al. [14].

In this paper, a new approach based on turbulent energy spectra is adopted to derive the continuous-turbulence modeling equation. The flow past a circular cylinder is simulated to test this approach. This represents the first time the continuous-modeling approach has been applied to a compressible, wall-bounded, or fully inhomogeneous turbulent flow. Because the relationship between the integral length scale (quantifying the larger energy-containing scales in the turbulence) and the mesh size is what controls the variation from RANS to LES model in the continuous-modeling approach, this flow provides an excellent opportunity to study the effect of changes in the integral length scale from one flow region to another on the behavior of the continuous model. In the next section, the continuous RANS–LES equations are derived. The numerical technique and results are reported in the third section. Conclusions are presented in the last section.

II. Derivation of a Continuous RANS–LES Model

Based on the assumption of the energy transport, which is local among all the scales of a turbulent flow, the average energy dissipation is the only parameter that describes the statistical properties far from the dissipation range. Kolmogorov [15,16] derived a universal scaling law of energy in the inertial range by dimensional analysis, $E(k) = C\epsilon^{2/3}k^{-5/3}$. With this energy scaling law, an intrinsic connection was established between the large scales and small scales. In the inertial range, turbulent eddies acquire continuous length scales. Consequently, a continuous kinematic eddy-viscosity model can be derived based on length scale and turbulent kinetic energy.

In terms of a turbulence length scale l and kinetic energy K, dimensional arguments dictate that the kinematic eddy viscosity ν_τ is given by

$$\nu_\tau = CK^{1/2}l \tag{1}$$

Assume that the turbulence is isotropic and follows the universal scaling law for $k' \ll k \ll k_\Delta$, as shown in Fig. 1. Thus, the preceding expression is valid for both large-scale (RANS) and subgrid-scale (LES) eddy viscosity. RANS is the case when $k \to k'$, and LES is the case when $k \to k_\Delta$, where k' is the wave number of the large energy-containing eddies and k_Δ is the cutoff wave number of the LES filter or grid filter. The length scales for RANS and LES are defined as L and Δ, respectively. Then for the RANS eddy viscosity, we have

$$\nu_\tau^{\mathrm{RANS}} = CK_L^{1/2}L \tag{2}$$

and for the LES eddy viscosity, we have

$$\nu_\tau^{\mathrm{LES}} = CK_\Delta^{1/2}\Delta \tag{3}$$

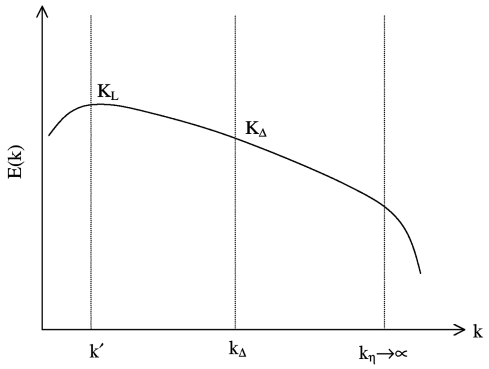

Fig. 1 Relative positions of RANS and LES scales on energy spectra.

The turbulent kinetic energy should reflect the dynamics of all modeled turbulence scales. Figure 1 shows the turbulence energy spectrum in the range from the largest eddies k' with length scale L up to the Kolmogorov scale k_η, where $k_\eta \to \infty$. RANS corresponds to modeling all scales from k' to k_η, and LES corresponds to modeling scales from the filtered scale k_Δ to the Kolmogorov scale k_η. To determine the modeled kinetic energy for each case, the integration should be performed through all modeled scales for RANS and LES, respectively. Therefore, for RANS, taking the integration from k' to k_η, we have

$$K_L = \int_{k'}^{\infty} E(k)\mathrm{d}k \tag{4}$$

For LES, taking the integration from k_Δ to k_η, we have

$$K_\Delta = \int_{k_\Delta}^{\infty} E(k)\mathrm{d}k \tag{5}$$

where $E(k)$ is prescribed by Kolmogorov's universal scaling law as

$$E(k) = C_k\epsilon^{2/3}k^{-5/3} \tag{6}$$

Using the relations $k' = 2\pi/L$ and $k_\Delta = 2\pi/\Delta$ gives the following equations:

$$K_L = \int_{2\pi/L}^{\infty} E(k)\mathrm{d}k = \frac{3C_k}{2}\epsilon^{2/3}L^{2/3} \tag{7}$$

$$K_\Delta = \int_{2\pi/\Delta}^{\infty} E(k)\mathrm{d}k = \frac{3C_k}{2}\epsilon^{2/3}\Delta^{2/3} \tag{8}$$

We finally derive, from all of the preceding equations, a relation between ν_τ^{LES} and ν_τ^{RANS}:

$$\nu_\tau^{\mathrm{LES}} = f(\Delta)\nu_\tau^{\mathrm{RANS}} \tag{9}$$

where

$$f(\Delta) = \left(\frac{\Delta}{L}\right)^{4/3} \tag{10}$$

Equation (9) prescribes the relationship between the RANS eddy viscosity and the LES eddy viscosity. The eddy-viscosity ratio is uniquely determined by a power law of the length-scale ratio. Because the integral length scale L represents the mean flow characteristic, a mixing-length hypothesis can be used to calculate this length scale L. (Note that although this use of a variable integral length scale accommodates the large-scale inhomogeneity of the flow, no attempt is made here to deal directly with the commutation error inherent in the application to inhomogeneous flows of viscosity formulas derived for homogeneous flows.) The integral length scale is assumed to be the same as the mixing length. For a far-wake flow, the mixing length is approximated to be proportional to the half-width of the wake:

$$L = l_{\text{mix}} = \alpha\delta(x) \tag{11}$$

According to some experimental data of flow past a circular cylinder, the value of the coefficient α can be calculated to be around 0.18. And the wake half-width grows according to

$$\delta(x) \approx 0.805\sqrt{x} \tag{12}$$

To make a correction of the length scale at the origination $x = 0$, we add a constant to Eq. (11). That is,

$$L_{\text{mix}} = \alpha\delta(x) + C \tag{13}$$

A relation similar to Eq. (10) was derived by Sagaut et al. [14] and Hussaini et al. [13], by means of a dimensional analysis argument and other assumptions. Using this relation, the subgrid-scale-model eddy viscosity can be calculated through the RANS equations. The RANS model can be either an algebraic model, a one-equation model, or a two-equation model. The base model used in the current study is the Spalart–Allmaras [17] RANS model. The continuous model provides a unified treatment of RANS and LES in turbulence simulations. As $\Delta \to L$, the RANS eddy viscosity is recovered, and as $\Delta \to \eta$, DNS is approached. For LES, Δ may be chosen to be the filter width or grid size. In practical applications, Δ is determined by the local mesh size. Therefore, a unified simulation of RANS and LES can be achieved by controlling the mesh distribution throughout the computational domain.

This development employed Kolmogorov's scaling law for the spectral energy distribution, which was used as the means for determining the change in K with scale and thus defined the nature of the interpolation between RANS and LES. Alternatives are certainly possible: an empirical fit to the energy-containing and lower-inertial-range parts of the energy spectrum, for example, could well be a better choice for those cases in which practical considerations do not permit a mesh fine enough for the inertial range. The relationship between Δ and grid size is also open to alternatives. The choice here was guided by the LES limit being essentially the Smagorinsky model, for which best results have generally been achieved when Δ is chosen in this fashion. A continuous model based on different RANS and LES models, however, might require a different choice.

III. Numerical Results with the Continuous RANS–LES Model

We consider the flow past a circular cylinder, for which some experimental results are available. The Favre-filtered, unsteady, compressible, nondimensional Navier–Stokes equations are solved in curvilinear coordinates. They are discretized on a multiblock overset mesh (see Fig. 2) with a fourth-order compact scheme for spatial differentiation and the Beam–Warming scheme for implicit time integration. Characteristic boundary conditions are applied at the inflow and outflow boundaries. The slip boundary conditions are applied on upper and lower boundaries, and periodicity is assumed in the spanwise direction. The standard message-passing interface is used for parallel computations on multiple zones. To maintain the stability of the scheme, a sixth-order compact filter is applied within each block. The details of the methodology are given by Uzun et al. [18,19].

The simulations are performed for Reynolds number 3900 and Mach number 0.3 on a coarse mesh and a fine mesh. The streamwise, normal, and spanwise dimensions of the background domain are 40, 20, and 2 diameters, respectively. The inflow boundary is 10 diameters upstream of the cylinder and the outflow boundary is 30 diameters downstream of the cylinder. Both the upper and lower boundaries are 10 diameters away from the center of the cylinder. For the coarse mesh, the body-block mesh resolution is $161 \times 81 \times 31$ in the azimuthal, radial, and spanwise directions, respectively, and the wake-block resolution is $81 \times 161 \times 31$. For the fine mesh, the body-block mesh resolution is $241 \times 81 \times 61$ and the wake-block resolution is $121 \times 161 \times 61$. For both meshes, the body block extends in the streamwise direction from $x/D = 0.5$ to 1.5 and the wake block extends from $x/D = 1.0$ to 10, where D is the diameter

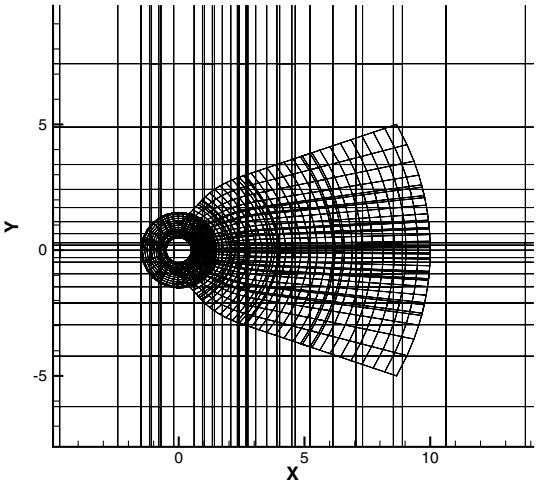

Fig. 2 Cylinder oversetting mesh.

of the cylinder. For the body blocks of both the coarse and fine meshes, the normal distance of the first point from the cylinder body is $\Delta_x = 1 \times 10^{-4}$ and the mesh size at the outer boundary is $\Delta_x = 1.8 \times 10^{-2}$, with a hyperbolic tangential distribution between the body surface and the outer boundary. For the wake blocks, the mesh changed from $\Delta_x = 2 \times 10^{-2}$ to 0.1. The mesh is uniformly distributed in the spanwise direction with $\Delta_z = 0.067$ for the coarse mesh and $\Delta_z = 0.04$ for the fine mesh. Natural instabilities in the flow initiated an unsteady solution; the imposition of unsteady forcing or freestream unsteadiness was not required to start the solution. (Linearly stable flows, such as pipe flows, do require such techniques.)

To perform a quantitative analysis of the continuous model, both mean flow and turbulence statistics are compared with experimental data. The experimental data were obtained by Ong and Wallace [20] via hot-wire measurements at the Reynolds number $Re = 3900$. In the present computation, statistics were accumulated over approximately 10 vortex-shedding cycles ($T = 50D/U_\infty$), after the flow reached a statistically steady state. The flow quantities were also averaged over the periodic spanwise direction. As can be seen in the derivation of the continuous model, the integral length scale L is an important parameter of the model; its influence on the numerical results is examined in the current study. Both constant L and computed L based on the mixing-length model will be used in the computations.

Figure 3a shows the centerline streamwise mean velocity computed using the continuous model with $L = 1.0$ and 0.25 on the coarse mesh. The simulation results are compared with those from both the experiment and RANS simulation. The centerline mean velocity given by the continuous model on coarse mesh shows reasonable agreement with the experimental result in the near-wall region. The mean velocity value given by the continuous model is a bit lower than the experimental value in the region downstream of $x/D = 4.0$. We attribute this difference to the influence of compressibility and slip wall. Figure 3b shows the transverse mean streamwise velocity profiles at different axial stations $x/D = 1.06$, 1.54, and 2.02. It is observed that the widths of the wake at all stations are captured well with continuous-model simulations, even though some differences from the experimental results can be observed for the peak values, due to the inaccuracy of the centerline velocity. All in all, the mean velocities captured by the continuous-model simulation are comparable with those by RANS computations, with some improvements in the reverse-flow region. Figures 4a and 4b show the cylinder wake vorticity isosurface with continuous modeling at $L = 0.25$ and RANS modeling, respectively. Obviously, continuous modeling can capture more delicate vortex structures in the wake.

To compare the turbulence statistics, the Reynolds stresses are plotted at the stations $x/D = 3.0$, 4.0, 6.0, and 7.0 in Figs. 5 and 6 with coarse-mesh computations. Figure 5 shows the normal stress τ_{xx}, and Fig. 6 shows the shear stress τ_{xy}. Normal stresses usually

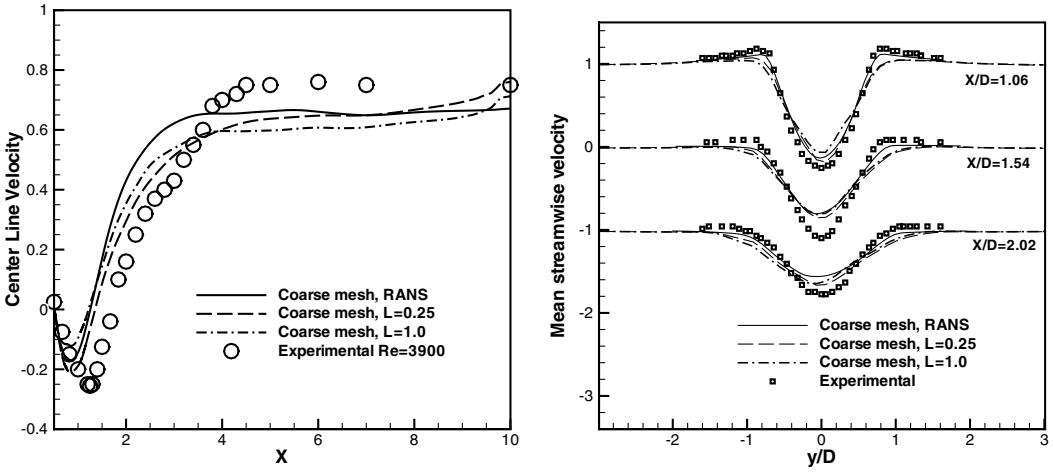

a) Centerline velocity **b) Streamwise velocity profiles**

Fig. 3 Mean streamwise velocity on coarse mesh.

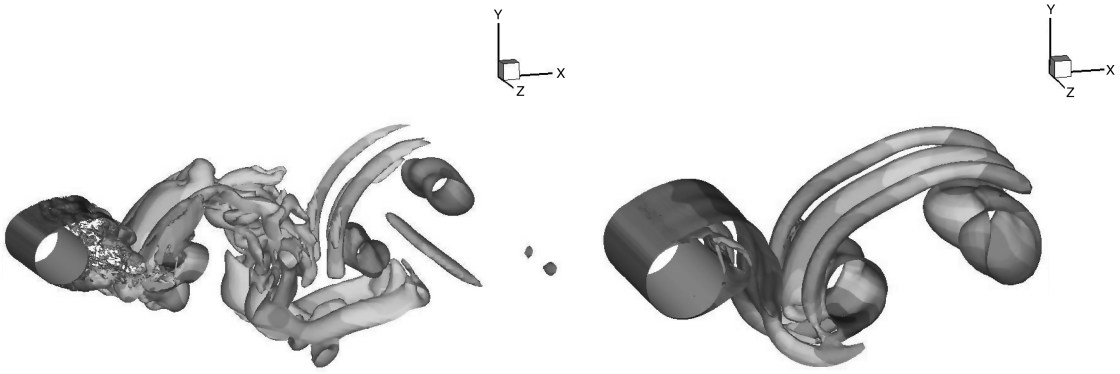

a) Continuous modeling **b) RANS modeling**

Fig. 4 Wake vorticity with coarse mesh.

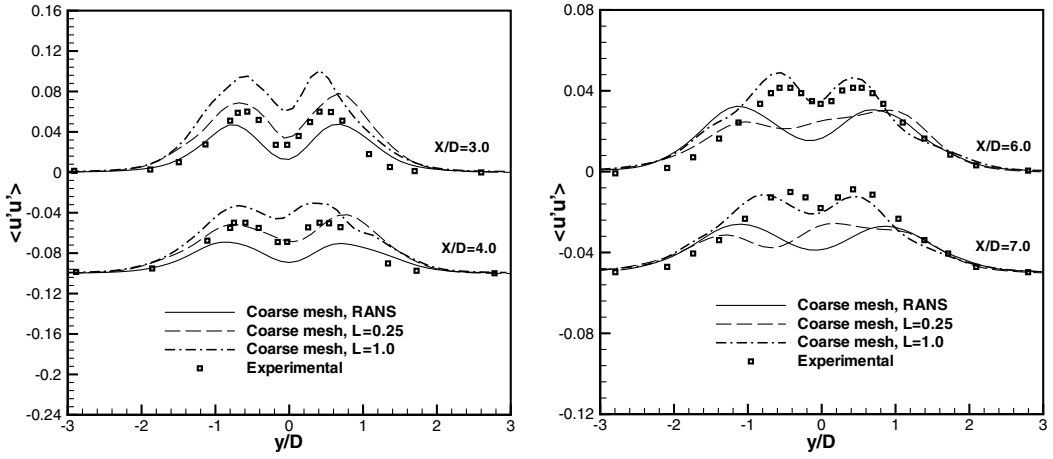

a) Near-wake stations **b) Far-wake stations**

Fig. 5 Normal stresses on coarse mesh.

reflect the turbulent intensities. From Fig. 5, it is observed that, compared with the experimental data, the normal stress is captured accurately by the continuous model with $L = 0.25$ at the stations $x/D = 3.0$ and 4.0 and with $L = 1.0$ at the stations $x/D = 6.0$ and 7.0. The normal stress is overestimated by the continuous model with $L = 1.0$ at the stations $x/D = 3.0$ and 4.0 and is underestimated with $L = 0.25$ at the stations $x/D = 6.0$ and 7.0. This indicates that the integral length scale L is a spatially dependent variable in the continuous model. The integral length scale is much smaller in the near-body wake than in the far wake. This is understandable physically, because the largest eddy size in the near-body wake is smaller than that in the far-wake area. Obviously, RANS computations

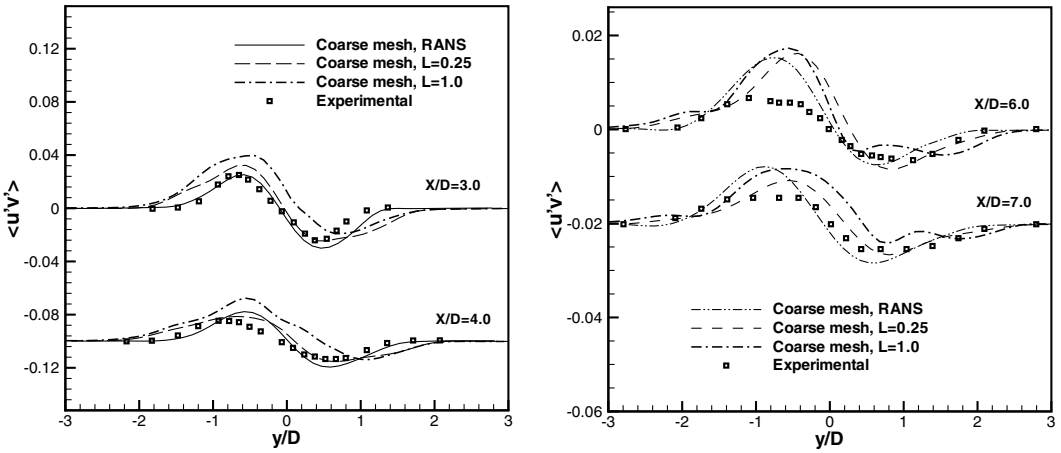

a) Near wake stations b) Far wake stations

Fig. 6 Shear stresses on coarse mesh.

underestimated the normal stresses at all locations because of large dissipation. The influence of the parameter L on the shear stresses shown in Figs. 6 is not as significant as on the normal stresses. $L = 0.25$ attains better agreements with the experimental results at most stations. The largest difference between the shear stresses computed with $L = 1.0$ and 0.25 is about 30%. A big deviation from the experimental results can be observed at $x/D = 6.0$. This may due to the coarse mesh used for these simulations.

For the simulations on the fine mesh with the continuous model, both constant L and spatially varied L estimated with the mixing-length model in Eq. (13) are studied. To compare with the constant L results, the constant C in Eq. (13) is set to be 0.1 so that the integral length scale has a value of around 0.25 at near-wake stations $x/D = 3.0$ and 4.0. Figure 7 shows the mean velocity with $L = 1.0$, 0.25, and L_{mix}. The mean flow results with the continuous model are comparable with the RANS results on the same fine mesh. The remarkable agreement with the experimental results for centerline velocity at $L = 0.25$ is observed in the reverse-flow region. The wake width at different stations is also computed accurately. Compared with those results on the coarse mesh shown in Fig. 3, the agreements with the experimental results are improved.

Figures 8 and 9 show the normal stresses and shear stresses computed on the fine mesh. It is observed that the turbulence statistics are less sensitive to the variation of integral length scale. The difference in normal stresses with $L = 0.25$ and 1.0 is relatively small at the near-wake stations $x/D = 3.0$ and 4.0. And good agreement with experimental results is observed at these stations. This is likely because the ratio Δ/L is smaller in large regions of the flow domain for a given range of L when the mesh is finer; this tends to make more of the flow solution LES-like and thus more accurate, but unnecessary computational costs are incurred in those regions in which the coarse grid was adequate. However, at the far-wake stations $x/D = 6.0$ and 7.0, the normal stresses show some irregular bumps and kinks in the wake center, although the normal stresses computed with varied $L = L_{\text{mix}}$ demonstrate more regular shapes. Good agreement with the experiments at stations $x/D = 3.0$ and 4.0 are also achieved. Some deviation can be observed at stations $x/D = 6.0$ and 7.0. This may be due to the inaccuracy of the model parameters used in calculation of the integral length scale. The agreement could be improved by adjusting the parameters in the model. Again, the RANS model with the fine mesh underestimated the normal stresses at both near-wake and far-wake stations, with more significant dissipation effects observed at those far-wake stations. The influence of the integral length scale on the shear stresses in Fig. 9 is not as significant as on the normal stresses. However, some improvements can still be observed with the continuous-modeling computation by $L = L_{\text{mix}}$ at the near-wake stations $x/D = 3.0$ and 4.0.

The discussion of this section gives some indication of the importance of the determination of the integral length scale on the solution and the change in the solution as the mesh is refined. The variable-length-scale concept employed here (using the mixing length) may readily be generalized for better accuracy. The length scale implicit in whatever RANS model is being used could be

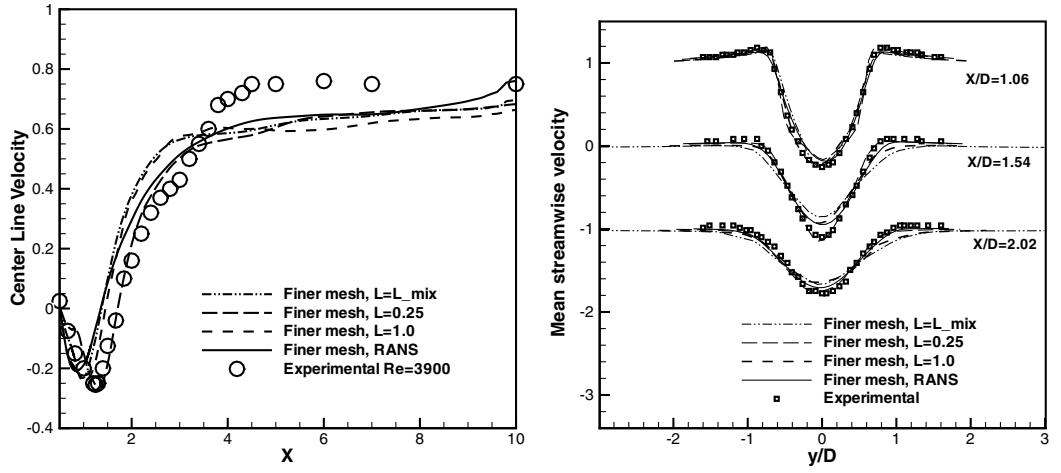

a) Centerline velocity b) Streamwise velocity profiles

Fig. 7 Mean streamwise velocity on finer mesh.

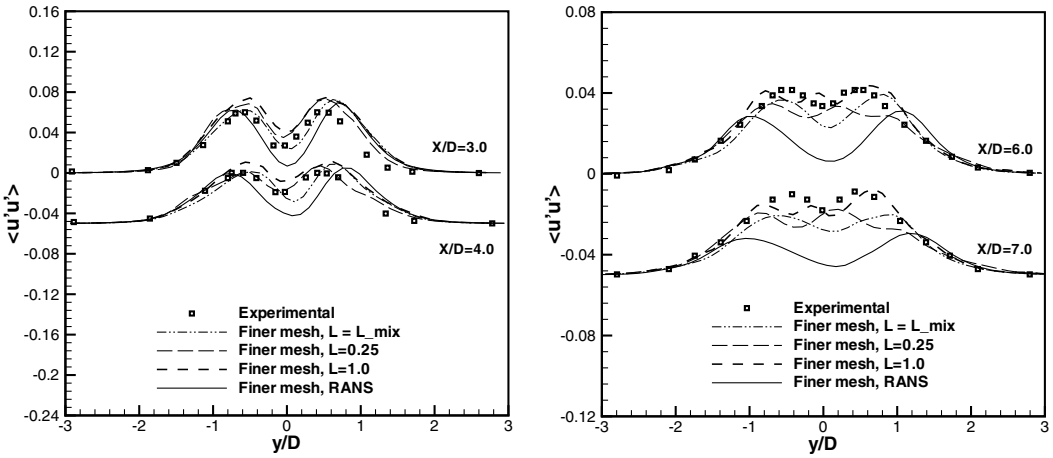

a) Near wake stations b) Far wake stations

Fig. 8 Normal stresses on fine mesh.

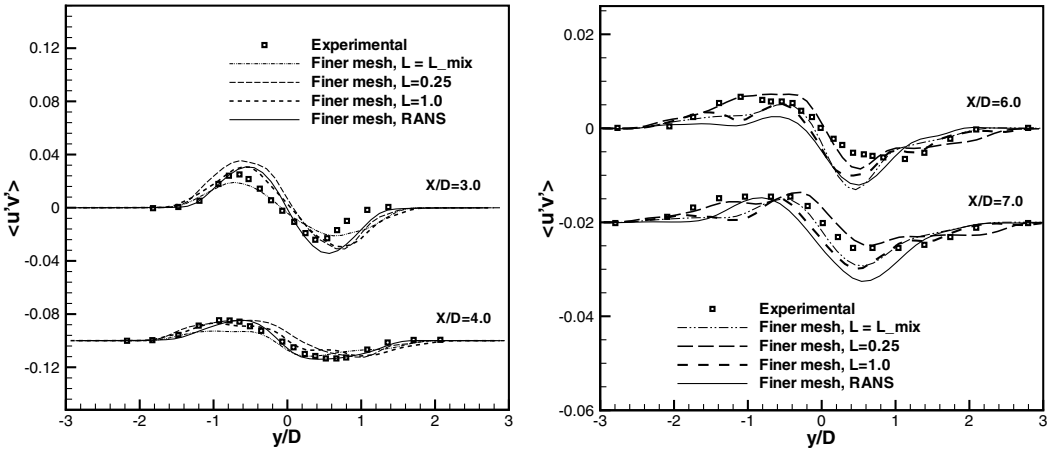

a) Near-wake stations b) Far-wake stations

Fig. 9 Shear stresses on fine mesh.

employed or more sophisticated means for extracting the length scale from the velocity field itself could be implemented, such as through the direct computation of the integral length scale. The finer mesh improved the solution in general, but in some parts of the flow, the coarser mesh, with its RANS solution, was perfectly adequate and the finer mesh served only to confirm this fact. In some parts of the flow, the coarse mesh was clearly inadequate, as indicated by the lopsided predictions for the shear stress in Fig. 5b, but in other parts, the solution looked reasonable but differed markedly from the experimental results (Fig. 3). As always, the final judgment on solution correctness is up to the experience and insight of the analyst.

IV. Conclusions

The continuous-modeling approach, based on the universal energy scaling law to bridge the turbulence scales from the large energy-containing eddies to the small subgrid eddies, may be employed to successfully simulate the unsteady turbulent flow past a circular cylinder at $Re = 3900$. With appropriate mesh resolution, the mean flow quantities computed with the continuous model agree well with experimental measurements, even in the reverse-flow region. Comparison of turbulent fluctuation statistics with experimental results indicates that the integral length scale employed in the continuous model is spatially dependent: a smaller integral length scale provides better results in the near-body wake region, whereas a larger integral length scale gives better results in the far-wake region. However, with refinement of the mesh, the turbulence statistics become less sensitive to this spatial dependence of the integral length scale. This is to be expected, because the finer mesh makes the continuous model more like an LES computation in more of the flow domain. Use of a spatially varying integral length scale, based on the mixing length, significantly improves the computational results.

Acknowledgments

Financial support for this work was provided by NASA Langley Research Center and NASA John H. Glenn Research Center at Lewis Field. The authors thank the technical monitors, David Lockard and Nick Georgiadis, for their encouragement and support. The authors also wish to thank the referees for their helpful suggestions.

References

[1] Speziale, C. G., "Analytical Methods for the Development of Reynolds Stress Closures in Turbulence," *Annual Review of Fluid Mechanics*, Vol. 23, 1991, pp. 107–157. doi:10.1146/annurev.fl.23.010191.000543

[2] Hussaini, M. Y., "On Large Eddy Simulation of Compressible Flow," AIAA Paper 1998-2802, 1998.

[3] Quemere, P., and Sagaut, P., "Zonal Multi-Domain RANS/LES Simulations of Turbulent Flows," *International Journal for Numerical Methods in Fluids*, Vol. 40, 2002, pp. 903–925. doi:10.1002/fld.381

[4] Labourasse, B., and Sagaut, P., "Reconstruction of Turbulent Fluctuations Using a Hybrid RANS/LES Approach," *Journal of Computational Physics*, Vol. 182, No. 1, 2002, pp. 301–336. doi:10.1006/jcph.2002.7169

[5] Terracol, M., "A Zonal RANS/LES Approach for Airframe Trailing-Edge Noise Prediction," *Euromech Colloquium 467: Turbulent Flow and Noise Generation*, Elsevier Science, Oxford, July 2005, pp. 18–20.

[6] Georgiadis, N., "Hybrid Reynolds-Averaged Navier-Stokes/Large Eddy Simulations of Supersonic Turbulent Mixing," *AIAA Journal*, Vol. 41, No. 2, 2003, pp. 218–239. doi:10.2514/2.1934

[7] Schluter, J. U., Wu, X., Kim, S., Shankaran, S., Alonso, J., and Pitsch, H., "A Framework for Coupling Reynolds-Averaged with Large Eddy Simulations for Gas Turbine Applications," *Journal of Fluids Engineering*, Vol. 127, 2005, pp. 806–815. doi:10.1115/1.1994877

[8] Spalart, P. R., "Strategies for Turbulence Modeling and Simulations," *International Journal of Heat and Fluid Flow*, Vol. 21, No. 3, 2000, pp. 252–263. doi:10.1016/S0142-727X(00)00007-2

[9] Spalart, P. R., Jou, W. H., Strelets, M., and Allmaras, S. R., "Comments on the Feasibility of LES for Wings, and on a Hybrid RANS/LES Approach," *Proceedings of the First AFOSR International Conference on DNS/LES*, Greyden, Columbus, OH, 1997, pp. 137–147.

[10] Spalart, P. R., "Trends in Turbulence Treatments," AIAA Paper 2000-2306, 2000.

[11] Travin, A., Shur, M., and Spalart, P., "Detached-Eddy Simulations Past a Circular Cylinder," *Flow, Turbulence and Combustion*, Vol. 63, 1999, pp. 293–313.

[12] Speziale, C. G., "A Combined Large Eddy Simulation and Time-Dependent RANS Capability for High-Speed Compressible Flows," *Journal of Scientific Computing*, Vol. 13, No. 3, 1998, pp. 253–274. doi:10.1023/A:1023266932231

[13] Hussaini, M. Y., Thangam, S., Woodruff, S. L., and Zhou, Y., "Development of a Continuous Model for Simulation of Turbulent Flows," *Journal of Applied Mechanics*, Vol. 73, No. 3, 2006, pp. 441–448. doi:10.1115/1.2173006

[14] Sagaut, P., Deck, S., and Terracol, M., *Multiscale and Multiresolution Approaches in Turbulence*, Imperial College Press, London, 2006.

[15] Kolmogorov, A. N., "The Local Structure of Turbulence in Incompressible Viscous Fluid at High Reynolds Number," *Doklady Akademii Nauk SSSR*, Vol. 30, 1941, pp. 299–303.

[16] Kolmogorov, A. N., "A Refinement of Previous Hypothesis Concerning the Local Structure of Turbulence in a Viscous Incompressible Fluid at High Reynolds Number," *Journal of Fluid Mechanics*, Vol. 13, 1962, pp. 82–85. doi:10.1017/S0022112062000518

[17] Spalart, P. R., and Allmaras, S. R., "A One-Equation Turbulence Model for Aerodynamic Flows," *La Recherche Aérospatiale*, Vol. 1, No. 5, 1994, pp. 5–21.

[18] Uzun, A., and Hussaini, M. Y., "Noise Generation in the Near-Nozzle Region of a Chevron Nozzle Jet Flow," AIAA Paper 2007-3596, 2007.

[19] Uzun, A., Hussaini, M. Y., and Streett, C. L., "Large Eddy Simulation of a Wing Tip Vortex on Overset Grids," *AIAA Journal*, Vol. 44, No. 6, 2006, pp. 1229–1242. doi:10.2514/1.17999

[20] Ong, L., and Wallace, J., "The Velocity Field of the Turbulent Very Near Wake of a Circular Cylinder," *Experiments in Fluids*, Vol. 20, No. 6, 1996, p. 441.

P. Givi
Associate Editor